Look-up table based Monte Carlo inverse model as a tool to discover liver tumors

Alexandra Andersson

2015

LUND UNIVERSITY
Faculty of Science

Alexandra Andersson
Bachelor thesis, Physics, 15 hp, Lund University
Supervisor: Nina Reistad, Atomic physics, Lund University
Co-supervisor: Stefan Andersson-Engels, Atomic physics, Lund University

Faculty of Science
Lund University
Lund 2015

Abstract

Diffuse reflectance spectroscopy is a method that allows investigation of the chromophore composition of tissue. The objective is to explore if the composition can be used to determine whether the tissue is healthy or not. The measured diffuse reflectance is often modelled by a diffusion model. However, the diffusion model has some shortcomings, and therefore this project uses a Monte Carlo model to analyse the measured spectrum. In this thesis a Look-up table based Monte Carlo inverse model is developed and compared to a diffusion model for measurements of *ex vivo* animal liver, *in vivo* human liver and measurements that investigate the effect of the probe pressure on the chromophore composition.

The results show that the Monte Carlo model is a promising method, but in its present form in need of some improvements. The pressure measurements show that a higher pressure results in increased diffuse reflectance. This can be explained by the result of the MC model, but since there are only few studies in this area with contradictory results, no solid conclusions can be drawn from this study.

Abbreviations

CRC	Colorectal cancer
DA	Diffusion approximation
DM	Diffusion model
DR	Diffuse reflectance
DRS	Diffuse reflectance spectroscopy
LUT	Look-up table
MC	Monte Carlo
MCLUT	Monte Carlo look-up table
MCML	Monte Carlo simulations for multi-layered media
NIR	Near infrared range
RTE	Radiation theory equation
SDS	Source detector separation
SUS	Skånes universitetssjukhus
VIS	Visible range

Symbols

mfp	Mean free path	(cm)
μ_t	Total attenuation coefficient	(cm^{-1})
μ_a	Absorption coefficient	(cm^{-1})
μ_s	Scattering coefficient	(cm^{-1})
μ_s'	Reduced scattering coefficient	(cm^{-1})
ρ	Source detector separation	(mm)
Δs	Step-size	(mm)
w	Photon package weight	-
a	Albedo	-
λ	Wavelength	(nm)
C_{diff}	Correction coefficient	-
B	Blood volume fraction	(%)
W	Water volume fraction	(%)
Bi	Bile volume fraction	(%)
L	Lipid volume fraction	(%)
S	Oxidation level	(%)
R_{vessel}	Vessel radius	(µm)
μ_a^{Hb}	Absorption coefficient for deoxygenated hemoglobin	(cm^{-1})
$\mu_a^{\text{HbO}_2}$	Absorption coefficient for oxygenated hemoglobin	(cm^{-1})
$\mu_a^{\text{H}_2\text{O}}$	Absorption coefficient for water	(cm^{-1})
μ_a^{Bile}	Absorption coefficient for bile	(cm^{-1})
μ_a^{Lipid}	Absorption coefficient for lipid	(cm^{-1})
P	Fraction Mie scattering	(%)
λ_0	Reference wavelength	(nm)
$\mu_s'(\lambda_0)$	Reduced scattering at 800 nm	(cm^{-1})
b	Scattering power coefficient	-
g	Anisotropy factor	-
θ	Scattering angle	(°)

Contents

Introduction

One of the leading underlying causes of death in the western world today is malignant tumours. In 2012, the amount of cancer cases was estimated to be 14.1 million, and the number of cases is expected to be around 24 million within 20 years. In 2012, the third most common cancer was colorectal cancer (CRC), with 9.7 % of all cancer diagnoses worldwide [1]. CRC is also the main reason for malignancies in the liver, (which was the sixth most common cancer type); as many as 30 to 50 % of the patients diagnosed with CRC developed liver malignancies [2, 3].

A common treatment of liver tumours is pre-operative chemotherapy combined with surgery. Pre-operative chemotherapy uses chemical substances that are sent into the tissue where it localizes and destroys the malignant cells while they are dividing. This reduces the tumour burden, which makes it possible for surgery where the tumours are resected. However, chemotherapy increases the risk of fatty liver diseases as steatosis and steatohepatitis [4].

Early detection of metastases and chemotherapy induced damages is a key to survival. Unfortunately, the only safe detection method of malignancies in the liver today is biopsies, which is a very time-consuming method. However, a previous study Volynskaya *et al*. [5] shows that metastases in the epithelial layer can be discovered by diffuse reflectance spectroscopy (DRS), which is a simple but effective method that investigates the diffuse reflectance (DR) of light illuminating tissue. Using DRS on liver tissue allows the possibility of diagnostics in real-time during surgery, which would be more time and cost-effective and thereby reduce the suffering of the patients and workload of the surgeons.

The DRS method has been evaluated on liver tissue in studies by e.g. Nachabé *et al*. [6], Evers *et al*. [7] , Reistad *et al*. [8] and Ahlburg and Kraus [9], where the diffusion equation by Farrell *et al*. [10], has been used as analysis model for the measured DR. However, the diffusion model (DM), has some limitations; the source detector separation (SDS, ρ) must be larger than the mean free path (*mfp*) so the photons have the opportunity to scatter, i.e. fulfil

$$\rho \gg mfp = \frac{1}{\mu_s' + \mu_a} = \frac{1}{\mu_t}, \tag{1}$$

where μ_t is the total attenuation coefficient being the sum of the absorption (μ_a) and reduced scattering (μ_s') coefficients. Further, the absorption coefficient must be much smaller than the scattering coefficient,

$$\mu_a \ll \mu_s', \tag{2}$$

or the light will be absorbed before scattered sufficiently to fulfil the diffusion approximation (DA). This is not always the case in liver tissue where blood is highly absorbing below 600 nm and water and bile are highly absorbing above 1400 nm (see Fig. 1).

Another method that can be used to analyse DR spectra is Look-up tables (LUT); either created using experimental measurements of tissue phantoms with known optical properties [11] or created by Monte Carlo (MC) simulations of photons in tissue. MC simulations has earlier been developed by Hennessy *et al*. [12] in shape of a LUT based inverse model. This model has no limitations on the absorption and reduced scattering coefficients, and has shown good results for wavelengths as short as 400 nm.

An interesting question during *in vivo* tissue measurements is to what extent the pressure on the tissue by the probe will influence the diffuse reflectance signal. It may also be necessary to avoid air between the probe and the tissue that can refract the light. A series of

increased pressure has been studied and evaluated with a DM by Reistad *et al*. [13], with the result that a higher pressure increases the DR below 590 nm and decreases the DR above 590 nm. Other studies by Randeberg [14], gives similar results, while a study by Chan *et al*. [15], shows that an increased pressure results in a decreased DR. That was explained by tissue compression that resulted in increased absorption and scattering.

The purpose of this bachelor project is to investigate MC simulations of the light propagation and a LUT based inverse model to analyse diffuse reflectance spectra from around 500 to 1500 nm as an alternative to the diffusion model. The MC model is then compared to the results of the DM using the analytical expression by Farrell *et al*. [10], for measurements of *in vivo* human as well as *ex vivo* bovine and porcine liver.

Since the effect of the probe pressure is an important factor, the analysis model must be able to detect probe pressure differences. Therefore, the two models will be compared for three different pressures.

Materials and methods

Diffuse reflectance spectroscopy

Diffuse Reflectance Spectroscopy (DRS) is a method where light is emitted into tissue through an optical fibre [16]. When illuminating tissue with light, the light will travel along certain paths in the tissue depending on the optical properties; the absorption coefficient, determining how far the light propagates in a medium before absorption, the refractive index and the reduced scattering coefficient, determining how far the light propagates in the medium before scattering. The absorption is due to different chromophores in the tissue. The chromophores absorbs different amount of light for different wavelength, yielding different light attenuation. The scattering is instead caused by variations in the refractive index within the tissue, and is also wavelength dependent, which result in different amounts of scattering for different wavelengths. The photons that are scattered and exits the tissue can then be collected by another optical fibre, resulting in a wavelength-dependent reflectance spectrum. The volume fractions of the chromophores differ from healthy tissue, tumours and chemotherapy induced damages, which results in different reflectance spectra. To assess the volume fractions of the chromophores, the measured spectrum must be modelled to a spectrum with known volume fractions.

Instrumentation and experimental setup

The experimental setup consists of a light-source, a fibre optical contact probe and two spectrometers connected to a computer with a program for data collection (Ocean View). The system (see Fig. 1) is mobile and easy to transport between the laboratory and the hospital, the two places where all measurements take place.
To emit light, a broadband Tungsten-Halogen light source, (Ocean Optics HL-2000-HP), is used to send out light from around 360 to 2000 nm through a custom designed 10-mm-diameter trifurcated fiber bundle probe. It is covered by a metallic cylinder and plastic at the end, to be able to be sterilized before each surgery. The fibre bundle is arranged with an illuminating fibre with a core diameter of 400 µm in the middle, and ten collecting fibres with a core diameter of 200 µm in a circle around the illuminating fibre. The

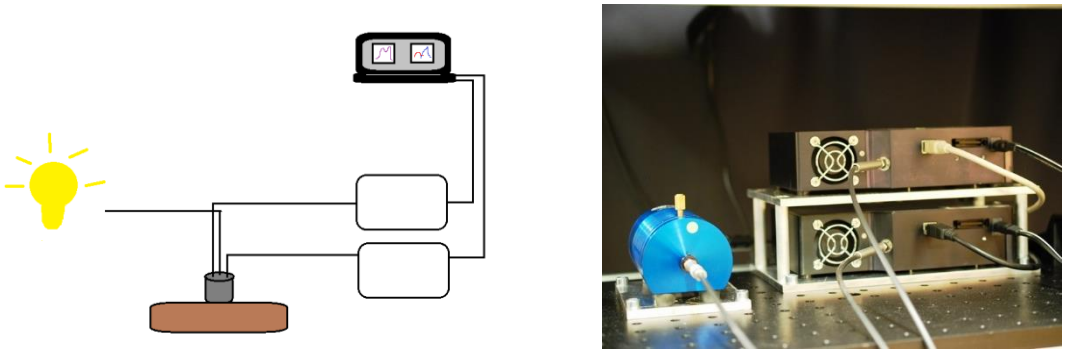

Figure 1. *Left* Sketch of the setup. The lamp is a symbol for the light source, the rectangles symbolises the spectrometer, the brown slice is the liver and the gray cylinder is the probe. *Right* Image of t of the setup. The blue half-cylinder is the light source and the black boxes are the spectrometers. Photo: Nina Reistad 2015.

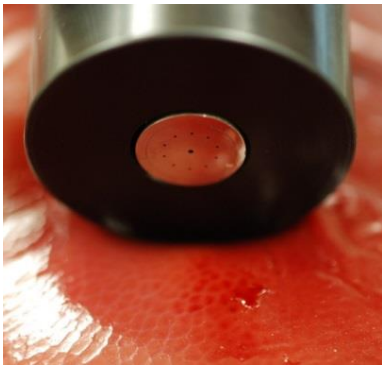

Figure 2. Image of the probe and the probe holder. Photo: N. Reistad 2015.

source-detector separation (SDS) between the illuminating and collection fibres is 2.5 mm, which gives a penetration depth of a couple of mm. It is important that the fibers are placed correctly and the probe is held perpendicular to the tissue, to avoid refraction and get as high intensity of the DR as possible. A sketch and picture of the probe with the probe holder can be seen in Fig. 2.

Every other collecting fibre in the probe are connected to a spectrometer in the visible (VIS) wavelength range, (Ocean Optics QE65000), and the others are connected to a spectrometer in the near infrared (NIR) range (Ocean Optics NIRQUEST512). The Ocean Optics QE65000, has a 100 µm slit and collects light in a range from 350 nm to 1000 nm. The Ocean Optics NIRQUEST has a 25 µm wide slit and covers a range from 900 to 1700 nm.

Measurements

Measurements are done both of *ex vivo* animal liver in the laboratory, *in vivo* human liver during surgeries at SUS and of *ex vivo* animal liver during so called probe pressure measurements. All human liver measurements were performed in accordance with approval from the regional Ethics Committee (EPN) in Lund.

Before the measurements start, the lamp is turned on around ten minutes before the measurements begin to let the temperature stabilize. The integration times of the NIR and VIS spectrometers are 20 and 5 ms, respectively. Background and intensity calibration spectra are saved by measuring the output signal when the probe is in contact with a spectrally flat white reflectance standard, (Spectralon, Labsphere, Inc., SRS-99-010), with the shutter closed and open, respectively. These spectra are used to calculate the measured DR,

$$R(\lambda) = \frac{S(\lambda)-B(\lambda)}{C(\lambda)-B(\lambda)}, \quad (3)$$

where $S(\lambda)$ is the raw tissue, $C(\lambda)$ is the calibration and $B(\lambda)$ is the background spectra.

The background and calibration measurements are done both before and after the measurements to compare against each other if there seem to be errors in the measurements. Common for all types of measurements is that it takes approximately twenty seconds in every point. During those twenty seconds, the DR is measured five times. i.e., five DR spectra are formed. If there are no errors, the five measured spectra are later formed to an average spectrum using Matlab.

Ex vivo measurements are done in ten random points of bovine and porcine liver during two sessions each. From these measurements, two spectra for each tissue type are randomly selected to be analysed.

During the *in vivo* measurements the probe is covered in a sterile surgical cover to avoid direct contact with the tissue and reduce the risk of infection. The probe is handled by the surgeon, who illuminates the tissue in 9 or 10 pre-determined points. The first 9 points are located in the same positions on the liver for every patient, and the 10th point is on the piece, supposed to be resected. If this piece is one of the 9 points, no 10th point is measured.

Several measurement sessions are conducted but only two of them are included in this evaluation. From each of the two sessions, two spectra are randomly chosen to be included in this thesis.

To study the effect of the probe-pressure, three different probe pressures, labeled hard, moderate and light and measured in unit of grams instead of Pa to make it convenient for the surgeons, are tested by one of the surgeons from SUS. The pressure measurements are done

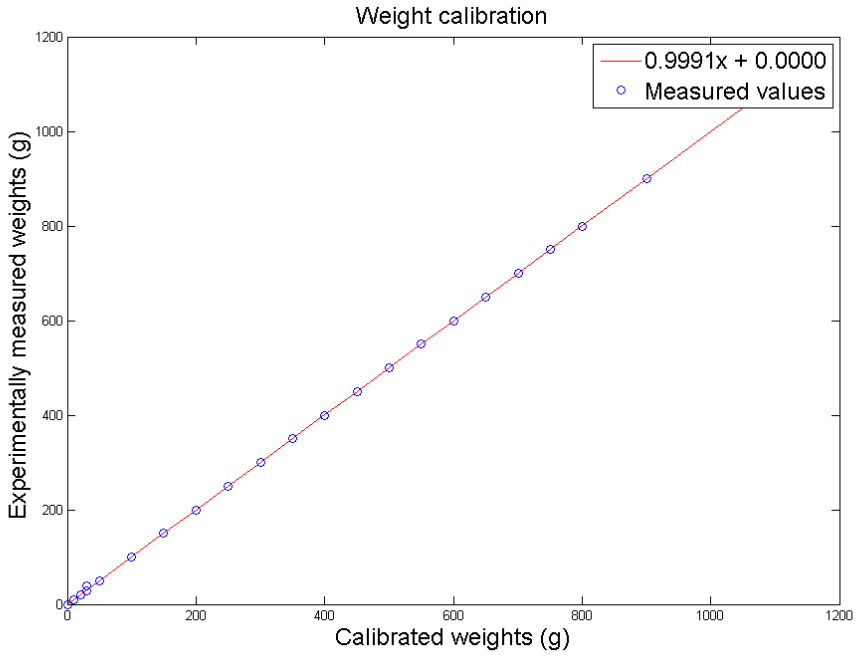

Figure 3. Experimentally measured weights as a function of calibrated weights.

twice with the surgeon to check the reproducibility, and a third time with an independent person who has never encountered the equipment before. The measurements are done of an *ex vivo* porcine liver placed on a weight scale, from which the pressure can be measured. To check the validity of the scale used, it is calibrated to a second scale with 100 time's higher precision, resulting in a linear relation. A plot of the relation between them can be seen in Fig. 3.

Modelling of the diffuse reflectance spectra

Previous studied by Bydlon *et al*. [16], and Jacques [17], have shown that the main absorbing chromophores in liver tissue are oxygenated are deoxygenated haemoglobin, lipids, water and bile, which are the chromophores that are considered in this thesis. Their absorption spectra, studied by Nachabé *et al*. [18], can be seen in Fig. 4.

The most important chromophores to study are oxygenated and deoxygenated haemoglobin, the two main chromophores in blood. Previous studies [19-21], show that the total concentration of haemoglobin and the oxidation level of the blood are two important indicators of malignant cells in breasts. Comparing healthy liver tissue with liver tumours, the tumours have almost six times higher oxidation level as the healthy tissue, according to a review by Bydlon *et al*. [16]. However, it should be noticed that the oxidation level does not give any information about the amount of oxygenated haemoglobin or total concentration of the blood itself, but only the ratio between them. In fact, tumours consist of less blood compared to healthy tissue. Further, it is important to separate values of the oxidation level of *ex vivo* and *in vivo* tissue. In *ex vivo* tissue, the oxidation level is about 5% to 10%, while in *in vivo* tissue; the oxidation level is 50% to 90%, depending on the investigated tissue.

Lipids are important to study since different types of lipids are the main components of cell membranes. A study by van Veen *et al*. [22] shows that lipids in general have an absorption peak around 900 nm. However, the review by Bydlon *et al*. [16], shows that this

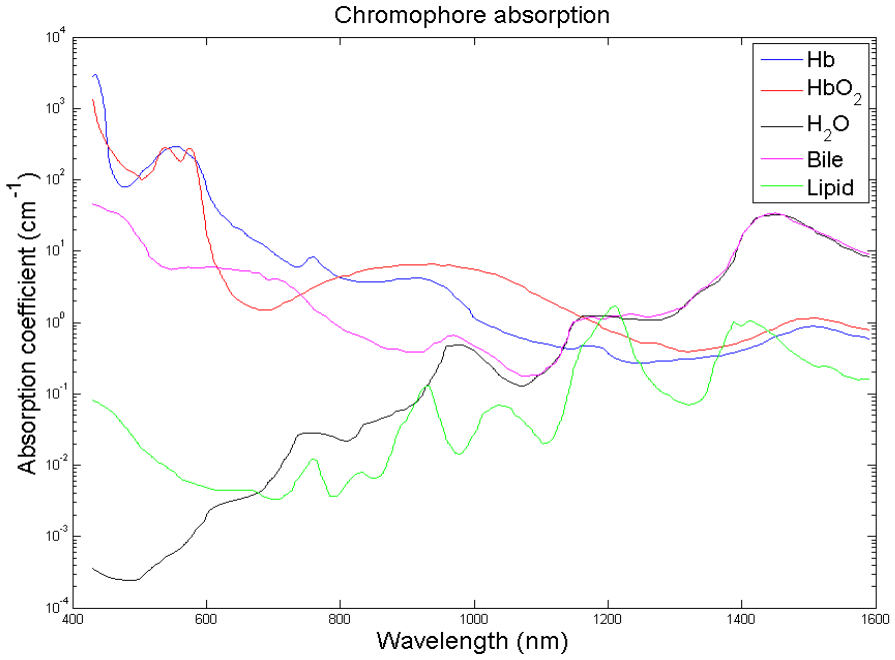

Figure 4. Absorption coefficients for the different chromophores as a function of wavelength. Data: Nachabé *et al*. [18].

absorption peak depends on the amount of saturated, monounsaturated or polyunsaturated fat. In this work, however, lipids are considered to be only one chromophore.

Water is the most common chromophore in human tissue. Since the absorption coefficient of water is insignificant in the visible wavelength range, water must be studied in the infrared wavelength range, where several absorption peaks in the range of interest in this thesis can be found.

Measurements by Nachabé *et al*. [6] show the importance of including bile as one of the absorbing chromophores concerning liver tissue. Not only does the bile absorption coefficient explain an earlier unexpected absorption peak in the diffuse reflectance spectra around 400 nm as well as an absorption plateau between 550 nm and 600 nm, but bile absorption can also be an indication of liver tumours since liver tumours have five times higher bile fraction than healthy liver tissue [16].

Analysis model

If the optical properties are known, the propagation of light in tissue can be modelled by the Radiative transfer equation (RTE), which is derived from five radiative processes. These five processes are:

1. gain of photons due to scattering from other directions,
2. gain of photons due to sources,
3. loss of photons due to absorption,
4. loss of photons due to scattering to other directions,
5. loss of photons due to escape out of the control volume.

However, the RTE is almost impossible to solve without approximations or simulations. In this thesis, MC-simulations, a stochastic method using deterministic algorithms, are used. A typical pattern of a MC simulation is:

1. definition of possible input parameters,
2. stochastically input parameters are generated from a probability density function,
3. deterministic computations of the input parameters,
4. termination of computations.

MC computations of photons simulate the path of the photon packages as they are absorbed and scattered in tissue [23]. When a photon package is launched into the tissue, it is moved a certain distance, given by a step-size that change depending on the mean free path. To get a realistic photon path, the step-size is stochastically simulated every time the photon package travels a new distance,

$$\Delta s = \frac{-ln\varepsilon}{\mu_t}, \tag{4}$$

where ε is a stochastic number between 0 and 1. When the photon package has moved a distance, it might have transmitted or been internally reflected out of the tissue. In that case, the happening is recorded, and a new photon package is launched.

If the photon package is still in the tissue, it is scattered. Every time the photon package is scattered, a small fraction of it is absorbed. Considering that the photon package has an initial weight *w*, the new weight is reduced to

$$w' = aw, \tag{5}$$

where *a* is the albedo,

$$a = \frac{\mu_s}{\mu_t}. \tag{6}$$

If the weight of the photon package is less than 0.1% of the initial photon package weight, it

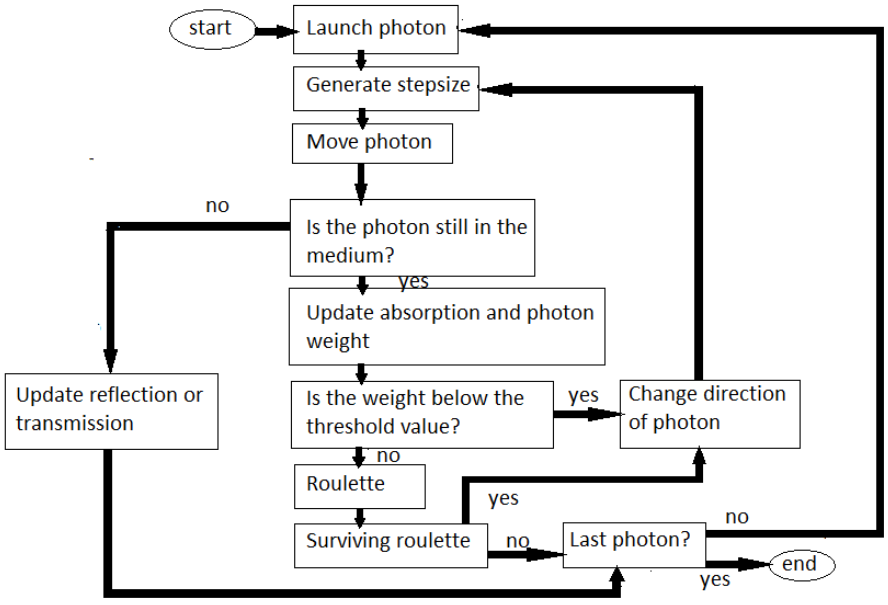

Figure 5. Flowchart of the forward and inverse model. Inspired by a flowchart by Hennessy *et al.* [12].

has to go through a so called roulette, where it has 10% chance of surviving. If the photon package survives the roulette, its weight is increased with a factor ten to conserve the energy in the system. In case the photon package survives, or simply has a weight over 0.1% of the initial weight, it continues its path in the tissue. If it is killed, the weight is reduced to zero and the next photon package is launched. This process continues until all photon packages are killed. The whole process can be seen in Fig. 5, a flowchart inspired by Hennessy *et al*. [12].

MC in tissue can be simulated by three different types of programs, White MC, CUDAMCML and MCML [24]. White MC is a single simulation of one combination of a reduced scattering coefficient and absorption coefficient set to zero. The result of the simulation is then used to predict the results from other combinations. The method can be used for both infinite and semi-infinite media, and is often used in time-resolved measurements.

CUDAMCML and MCML works in the same way, simulating the path of the photons for tissue with one or several layers with different optical properties. However, CUDAMCML can run simulations of many photon packages at the same time, using both the graphics card and the CPU of the device, while the regular MCML only runs one photon package at a time, only using the CPU.

During this thesis, a Multi-layered Monte Carlo, (MCML), program provided by Jacques and Wang. [25], and modified by Alerstam [24], will be used. The user can choose input parameters as absorption and reduced scattering coefficients, refractive index, anisotropy factor, thickness, and radius. The idea is to create a LUT with values of reflectance from different combinations of reduced scattering and absorption coefficients. Those combinations covers a region of interest, calculated by a forward model that uses initial chromophore volume fractions from Nachabé *et al*. [6]. The spectrum generated by those volume fractions will be optimized by an inverse routine that updates the input parameters until the squared differences between the spectra in every point is minimized. A flowchart, inspired by Hennessy *et al*. [12], of the different steps can be seen in Fig. 6.

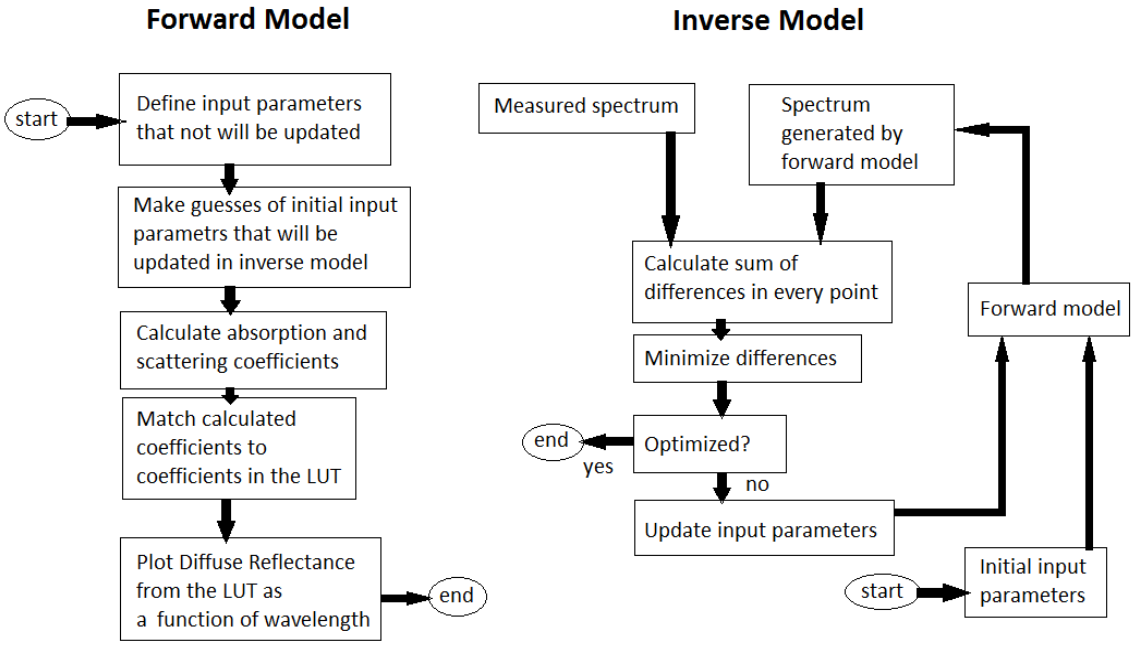

Figure 6. Flowchart of the forward and inverse model. Inspired by a flowchart by Hennessy *et al.* [12].

Forward model

The forward model creates wavelength-dependent combinations of absorption and reduced scattering coefficients. The absorption coefficient for the tissue can be described as a linear combination of the absorption coefficient for every chromophore,

$$\mu_a(\lambda) = C_{\text{diff}}(\lambda)B\left[S\,\mu_a^{HbO_2}(\lambda) + (1-S)\mu_a^{Hb}(\lambda)\right] + W\mu_a^{H_2O}(\lambda) + L\mu_a^{Lipid}(\lambda) + Bi\mu_a^{Bile}(\lambda). \quad (7)$$

Here, *B, W, L* and *Bi* are the volume fractions of blood, water, lipid and bile respectively and *S* is the oxidation level of the blood,

$$S = \frac{HbO_2}{Hb+HbO_2}, \quad (8)$$

where C_{diff} is a correction coefficient due to the inhomogeneity caused by the blood vessels, given by van Veen *et al*. [26],

$$C_{\text{diff}}(\lambda) = \frac{1-e^{-2R_{\text{vessel}}(S\,\mu_a^{HbO_2}(\lambda)+(1-S)\mu_a^{Hb}(\lambda))}}{2R_{\text{vessel}}(S\,\mu_a^{HbO_2}(\lambda)+(1-S)\mu_a^{Hb}(\lambda))}. \quad (9)$$

The absorption coefficients for the different chromophores and the blood vessel radius have been reported by Nachabé *at al*. [6], and are valid for wavelengths from 400 to 1600 nm, (Fig. 1). The volume fractions for the different chromophores, *S*, $\mu_s'(\lambda)$ and *b* used to calculate the scattering coefficients, are expectation values for a healthy *ex vivo* human liver, from an article by Nachabé *et al*. [6], and can be seen in Table 1. The calculated coefficients can be seen in Fig. 7. When the forward model is run later in the inverse model, the logarithm of the absorption coefficient is used, to match the LUT that is used.

Table 1. The input volume fractions, oxidation level, reduced scattering at 800 nm, scattering power coefficient, and fraction Mie scattering from Nachabé *et al*. [6], that generates the coefficients in Fig. 7.

Parameter	Values	Standard deviation
S (%)	8.0	14.0
W (%)	76.0	4.0
L (%)	16.0	3.0
Bi (%)	3.2	1.6
B (%)	5.5	2.3
$\mu_s'(\lambda)$ (cm^{-1})	17.0	3.0
b	1.2	0.7

Scattering of light in matter is due to differences in the refractive index of the medium. The scattering angle is most often described by the Henyey-Greenstein scattering probability function [23], which is a good approximation considering Mie scattering,

$$p(\theta) = \frac{1-g^2}{4\pi(1+g^2-2g\cos(\theta)^{\frac{3}{2}}}, \quad (10)$$

where g is the anisotropy factor

$$g = <\cos(\theta)>. \quad (11)$$

After a large number of scattering events, the information about the original directionality is lost and the light source is considered to be isotropic. One can therefore use the reduced scattering coefficient which describes the path of the photons in fewer steps, without losing any important information,

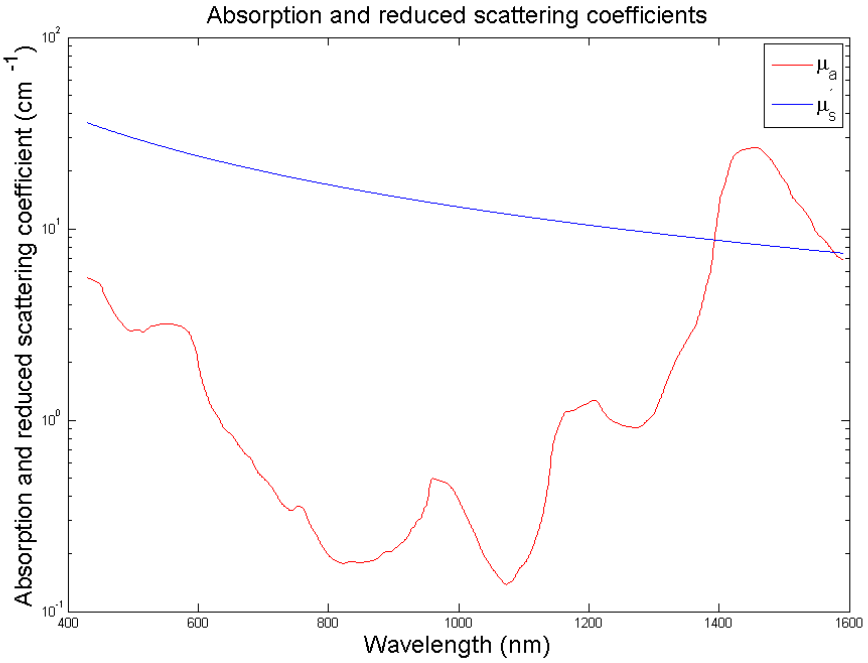

Figure 7. Absorption and reduced scattering coefficients as a function of wavelength. The coefficients are generated by the forward model, using input parameters given in Fig. 4 and Table 1. Data from Nachabé *et al.* [6].

$$\mu_s'(\lambda) = (1 - g) \cdot \mu_s \,. \tag{12}$$

Considering that the formula should not only be solved for certain wavelengths but a range of wavelengths from 430 to 1590 nm in accordance with a study by Nachabé *et al.* [18], the reduced scattering coefficient can be fit to two equations [17].

$$\mu_s'(\lambda) = \mu_s'(\lambda_0) \frac{\lambda}{\lambda_0}^{-b}. \tag{13}$$

$$\mu_s'(\lambda) = \mu_s'(\lambda_0) \left(p \frac{\lambda}{\lambda_0}^{-b} + (1 - \rho) \frac{\lambda}{\lambda_0}^{-4} \right). \tag{14}$$

The first (Eq. 13), concerns only Mie scattering and is used in the MC method, and the second (Eq. 14), includes both Mie and Rayleigh scattering and are used in the DM that are used as comparison.

Creation of Lookup-table

From Fig. 7, the regions of interest of the coefficients can be seen. Since there are a lot of variations of the absorption coefficient close to zero, an exponentially increasing absorption coefficient between 0.08 to 81.45 cm^{-1} in 70 steps are used to generate the LUT. The scattering coefficient is more linearly decreasing with a higher wavelength and is therefore linearly increased from 0 to 74 cm^{-1} in integer steps in the generation of the LUT. The values of the coefficients in the different steps can be seen in Fig. 8.

The LUT is generated by looping 100 000 photons over all possible combinations of coefficients, with a refractive index of the tissue is set to 1.4 and the *g*-factor set to 0.85. The thickness is set to be 100 cm to be thick enough to not let any photons being transmitted. The number of steps is set to 30 with a step-size of 0.1 mm. Since the only radius of interest is at

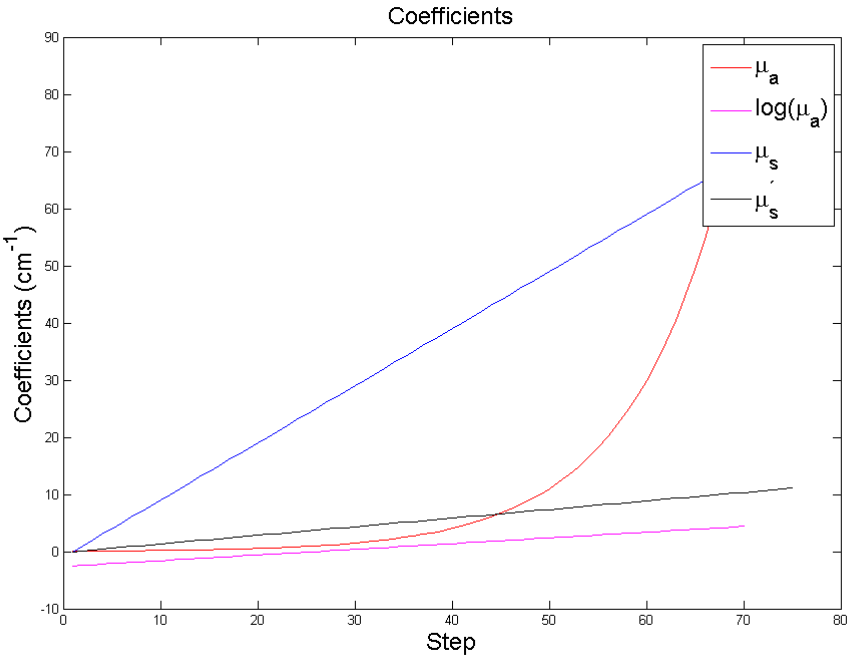

Figure 8. Values of absorption, logarithm of absorption, scattering and reduced scattering coefficients in the LUT and fit of the LUT as a function of their step.

2.5 mm to match the probe used in the measurements, the values for step 23 to 27 is saved as the DR in the LUT to get some margins. The resulting LUT is shown in Fig. 9.

Inverse model

To find the actual volume fractions the generated spectra must be iteratively changed to obtain a shape that resembles the measured spectrum as well as possible, and the initial input parameters from Table 1 updated correspondingly. This is done by a non-linear optimization routine in Matlab that uses the Levenberg-Marquardt algorithm. This routine takes the difference between the generated and measured spectra as a function and minimizes it.

The generated spectrum is calculated for integer number wavelengths in the range from 430 nm to 1590 nm. The measured spectrum, on the other hand, is dependent on decimal numbers in 1046 steps from 450.1 to 1549.4 nm, with different step-size due to the merging of the DR curves from the two different spectrometers. Since the optimization routine minimizes the difference between two points of the curves, the DR vectors have to be equally long and consider the same wavelength. Thus, an interpolation routine in Matlab is used that calculates the DR in the measured spectrum that corresponded to the integer wavelengths from the forward model from 575 to 1500 nm. Since the MCML gives DR in absolute values and the measured spectra are in relative units to the calibration spectra, the modelled spectra are normalized to the wavelength with highest DR in the measured spectra.

An analytical function is chosen to represent the MC-generated diffuse reflectance as a function of the step of the reduced scattering coefficient and the step of the logarithm of the absorption coefficients. This is solved by a polynomial fit of the LUT which is used in the inverse model. The LUT, its fit, and the residue of the fit can be seen in Fig. 9. The values of the different coefficients in every step in the LUT and the fit can be seen in Fig. 8. The coefficients for the polynomial are given in Table 2.

Table 2. Polynomial coefficients used in the polynomial function used as LUT in the inverse model. The first number after the P gives the degree of the logarithmic absorption coefficient, and the second number gives the degree of the reduced scattering coefficient.

P00	P10	P01	P20	P11	P02	P30
$9.521 \cdot 10^3$	$3.205 \cdot 10^3$	$8.546 \cdot 10^2$	$-1.640 \cdot 10^2$	$-9.490 \cdot 10^2$	$4.441 \cdot 10^2$	$3.194 \cdot 10^3$
P21	**P12**	**P03**	**P40**	**P31**	**P22**	**P13**
$6.215 \cdot 10^3$	$-1.132 \cdot 10^2$	$-7.291 \cdot 10^3$	$3.072 \cdot 10^3$	$6.799 \cdot 10^3$	$4.938 \cdot 10^4$	$1.751 \cdot 10^3$
P04	**P50**	**P41**	**P32**	**P23**	**P14**	**P05**
$4.150 \cdot 10^4$	$-7.379 \cdot 10^4$	$-8.649 \cdot 10^4$	$-1.389 \cdot 10^4$	$3.125 \cdot 10^5$	$-6.306 \cdot 10^5$	$-7.954 \cdot 10^6$

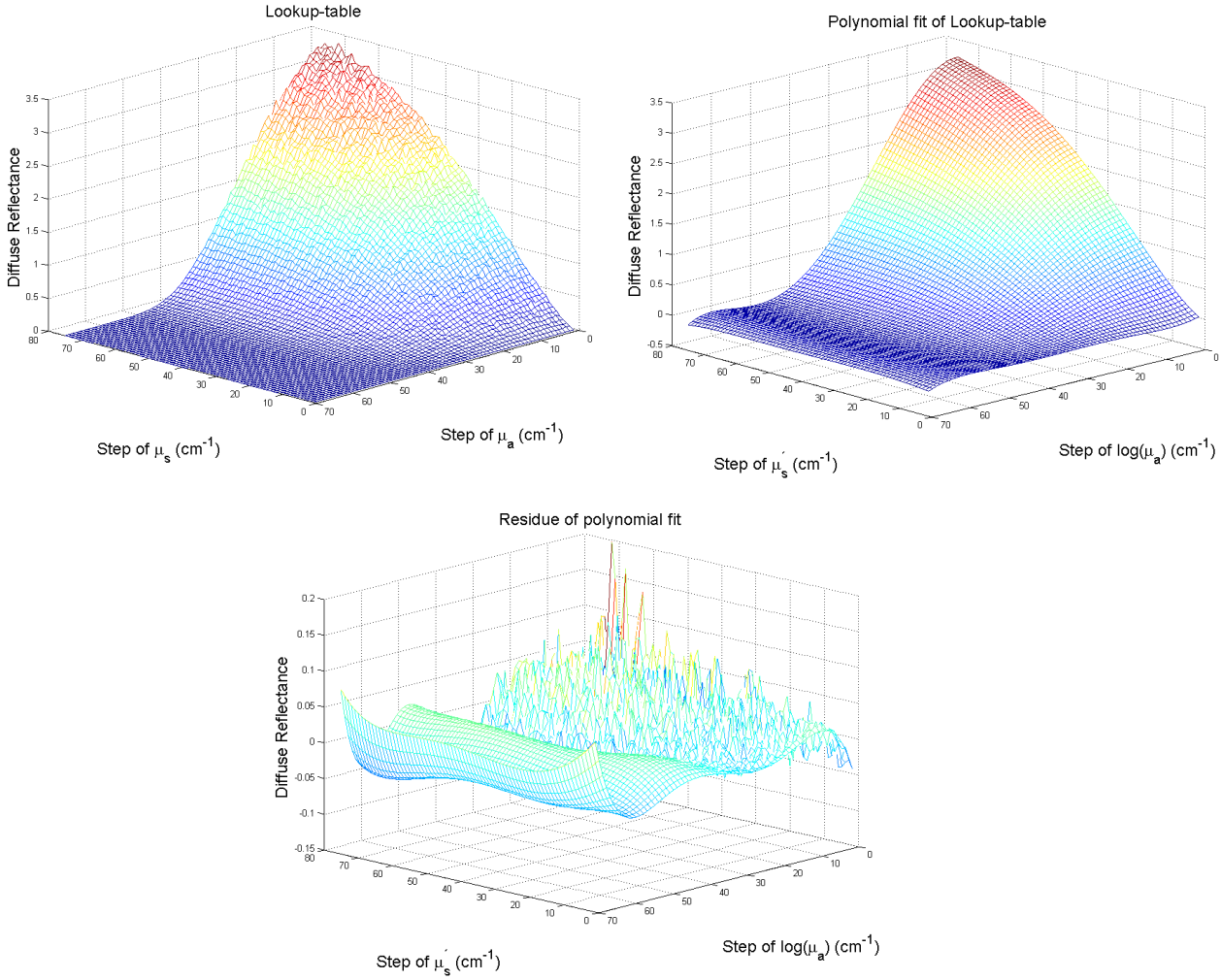

Figure 9. LUT gained by the MCML simulations. *Left:* Diffuse reflectance as a function of the steps of the scattering and the absorption coefficients. *Right:* Diffuse reflectance as a function of the step of the reduced scattering and step of the logarithm of absorption coefficients. Polynomial fit of the real LUT, which is used as LUT in the inverse model. *Botton:* Residue as a function of the step of the logarithm of the absorption and step of reduced scattering coefficients.

Results

Ex vivo bovine liver

The spectra chosen to be analysed from the *ex vivo* bovine measurements can be seen in Fig. 10. The figure shows the measured spectrum and the generated spectra from both the diffusion model and the MC model and their residues. Further, it shows that the two measured spectra are almost equivalent and that fit of the models are approximately equivalent, except between 700 and 1000 nm where the diffusion model has a better fit.

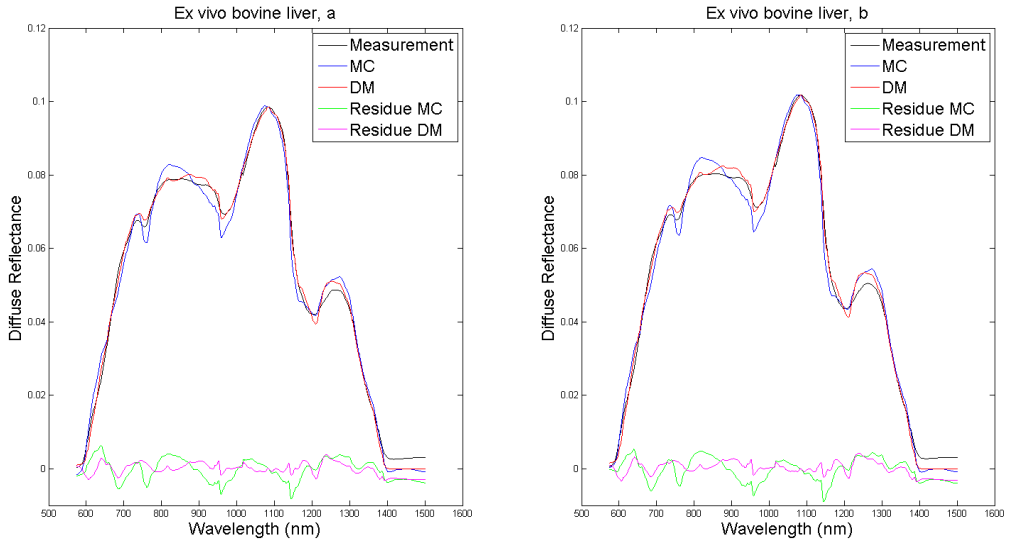

Figure 10. Diffuse reflectance as a function of wavelength. The plots show the measured spectrum, MC model, DM and their residues for the different points of *ex vivo* bovine liver.

Table 3. The updated volume fractions (*W*, *L*, *Bi*, *B*), oxidation level (*S*), reduced scattering at 800 nm ($\mu_s'(\lambda)$), scattering power coefficient (*b*), and fraction Mie scattering (ρ) for the spectra in Fig. 10.

Parameter	MC, a	DM , a	MC, b	DM, b
S (%)	11.9	80.1	14.8	83.8
W (%)	68.6	85.3	69.5	82.4
L (%)	14.1	37.2	14.1	36.3
Bi(%)	3.0	-	2.8	-
B (%)	8.6	11.9	8.6	11.0
$\mu_s'(\lambda)$ (cm^{-1})	12.8	16.1	12.1	16.2
b	0.3	3.4	0.2	3.4
ρ (%)	-	100.0	-	98.4
Total (%)	94.3	134.4	95.0	129.7

Ex vivo porcine liver

The spectra from the porcine measurements can be seen in Fig. 11. Just as for the bovine measurements, the measured spectra seem to be approximately equivalent in both points. The MC and DM fit are more similar than compared to the bovine liver since the DM fit have larger residues, which are concentrated between 700 and 100 nm, for both models.

The parameter values can be seen in Table 4.

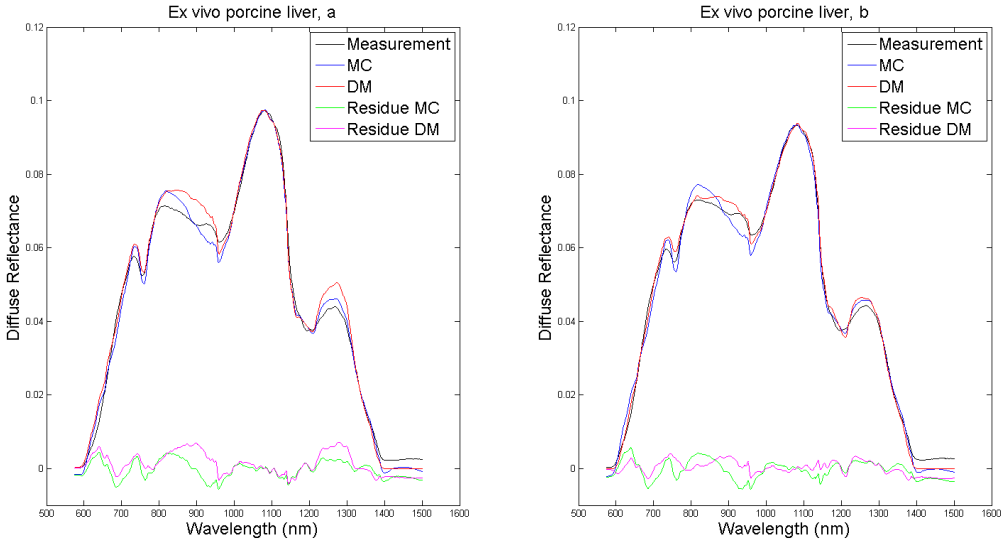

Figure 11. Diffuse diffuse reflectance as a function of wavelength. The plots show the measured spectrum, MC model, DM and their residues for the different points of ex vivo porcine liver.

Table 4. The updated volume fractions, oxidation level, reduced scattering at 800 nm, scattering power coefficient, and fraction Mie scattering for the spectra in Fig. 11.

Parameter	**MC, a**	**DM, a**	**MC, b**	**DM, b**
S (%)	16.9	16.7	11.4	66.0
W (%)	86.6	103.0	67.6	98.5
L (%)	21.1	20.4	16.9	35.9
Bi (%)	6.7	-	6.3	-
B (%)	19.8	9.9	11.2	12.8
$\mu_s'(\lambda)$ (cm^{-1})	8.3	14.7	22.4	13.1
b	1.0	0.6	1.1	3.1
ρ (%)	-	84.6	-	85.4
Total (%)	134.2	133.3	102.0	147.2

In vivo human liver

The spectra from the first *in vivo* measurement session can be seen in Fig. 12, and the spectra from the second session can be seen in Fig. 13. The spectra for each measurement occasion have quite different shape, which can be seen as differences in volume fractions in Table 5 and 6, for both the MC model and DM.

Both models seem to fit the measured spectra very well, but the DM fit has larger residues around 900 nm in some cases.

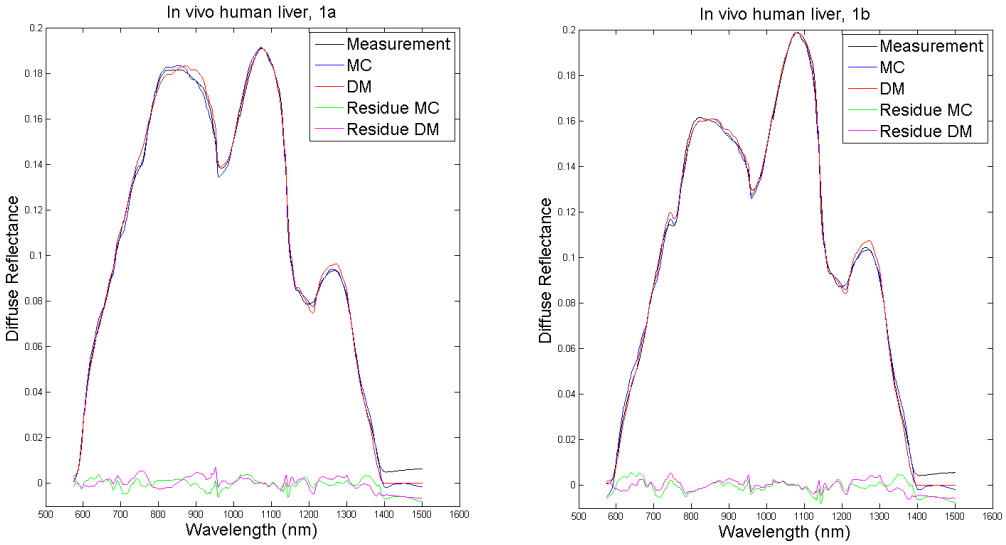

Figure12. Diffuse reflectance as a function of wavelength. The plots show the measured spectrum, MC model, DM and their residues for the different points from the first session of *in vivo* human liver.

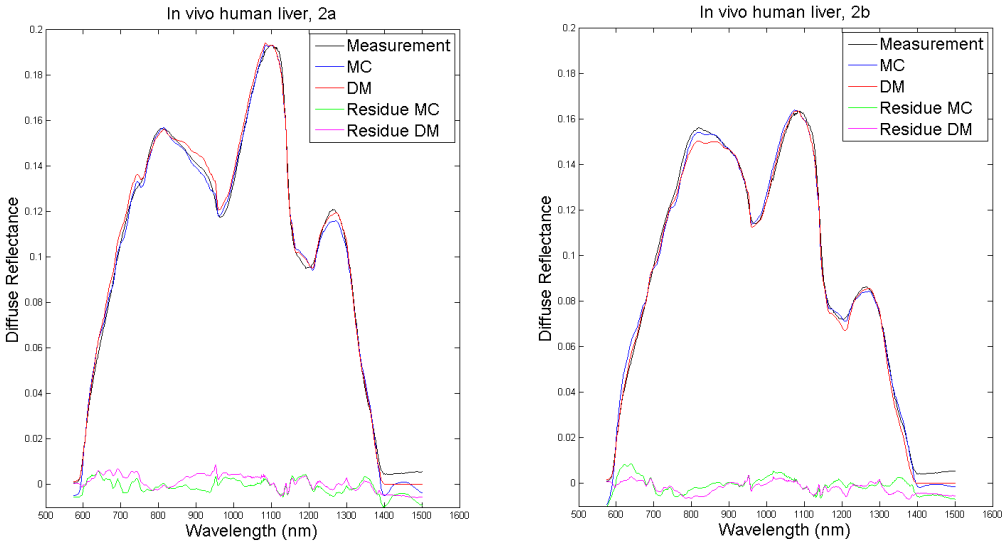

Figure13. Diffuse reflectance as a function of wavelength. The plots show the measured spectrum, MC model, DM and their residues for the different points from the second session of *in vivo* human liver.

Table 5. The updated volume fractions, oxidation level, reduced scattering at 800 nm, scattering power coefficient, and fraction Mie scattering for the spectra in Fig. 12

Parameter	MC,1a	DM,1a	MC, 1b	DM, 1b
S (%)	5.2	52.0	21.8	28.2
W (%)	60.9	90.1	58.2	83.6
L (%)	11.7	23.8	11.7	19.1
Bi (%)	13.0	-	15.8	-
B (%)	3.9	2.8	7.8	9.8
$\mu_s'(\lambda)\ (cm^{-1})$	14.4	13.6	12.9	10.7
b	0.5	1.7	0.3	0.8
ρ (%)	-	78.2	-	99.1
Total (%)	89.5	116.7	93.5	112.2

Table 6. The updated volume fractions, oxidation level, reduced scattering at 800 nm, scattering power coefficient, and fraction Mie scattering for the three spectra in Fig. 13.

Parameter	MC,2a	DM,2a	MC, 2b	DM, 2b
S (%)	58.8	65.2	29.6	57.8
W (%)	58.3	71.4	56.5	89.3
L (%)	15.0	14.1	10.1	20.1
Bi (%)	17.9	-	13.9	-
B (%)	13.1	9.9	4.5	5.4
$\mu_s'(\lambda)\ (cm^{-1})$	3.2	14.6	14.8	12.3
b	0.3	0.1	0.5	0.8
ρ (%)	-	80.1	-	74.9
Total (%)	104.3	95.4	85.0	114.8

Probe pressure measurements

The results of the variations of the pressures can be seen in Table 7. The two measurements with the surgeon show how much the pressure can vary between different days for the same person. To get an idea of how the pressures vary expectation values, standard deviations, and confidence intervals was made from all three sessions, as well as for the first two sessions combined. Even though the measurements are slightly different, the confidence intervals still overlap with each other and not with the higher or lower pressure interval.

Only the result from the first session is analysed with the MC and diffusion model, which can be seen in Fig. 14 and Table 8. A hard pressure has a high DR and vice versa, a result that the two first sessions had in common. The third session gave unfortunately no clear results.

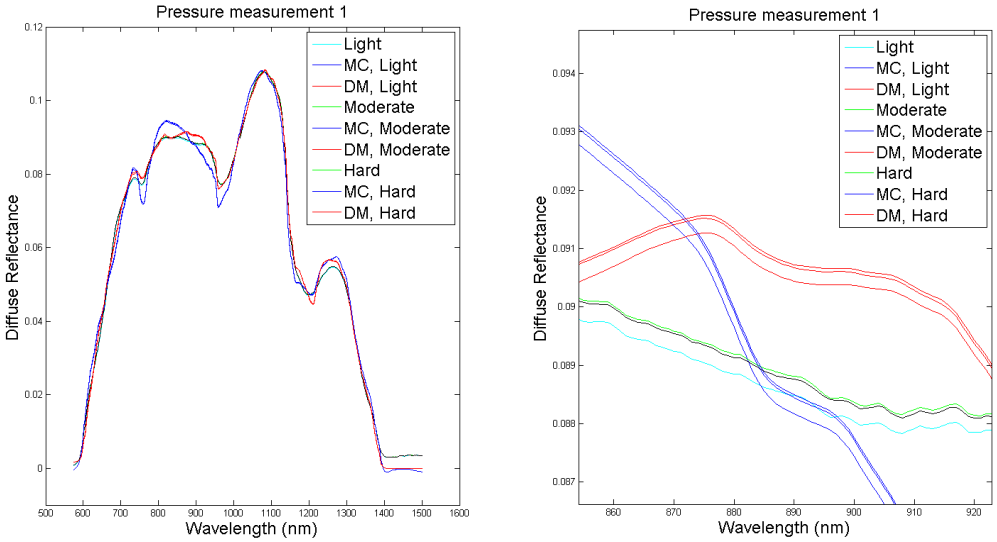

Figure 14. *Left.* Diffuse reflectance as a function of wavelength. The plots show the measured spectrum, MC model, DM for three different pressures on *ex vivo* porcine liver. *Right.* Normalized diffuse reflectance as a function of wavelength. Zoom of the left plot around 890 nm.

Table 7. Expectation values, standard deviations and confidence interval of 95% confidence level of the three different measurement sessions

Measurement	Pressure	Expectation value (g)	Standard deviation (g)	Confidence interval (g)
1	Light	27.75	8.31	24.11 – 31.39
1	Moderate	120.88	19.30	112.42 – 129.33
1	Hard	308.28	23.45	298.00 – 318.55
2	Light	34.30	24.52	23.99 – 44.61
2	Moderate	133.18	30.98	119.50 – 146.78
2	Hard	346.63	30.40	333.30 – 359.95
1 and 2	Light	31.03	17.72	25.53 – 36.52
1 and 2	Moderate	127.03	26.22	118.90 – 135.15
1 and 2	Hard	327.45	33.10	317.19 – 337.71
3	Light	9.65	5.08	7.42 – 11.88
3	Moderate	45.40	16.00	38.39 – 52.41
3	Hard	126.58	59.30	100.59 – 152.57

Table 8. The updated volume fractions, oxidation level, reduced scattering at 800 nm, scattering power coefficient, and fraction Mie scattering for the three spectra in Fig. 14.

Parameter	MC Light	DM Light	MC Moderate	DM Moderate	MC Hard	DM Hard
S (%)	10.2	79.5	9.7	80.6	9.7	78.8
W (%)	69.0	86.1	67.7	87.5	67.6	85.8
L (%)	11.5	32.1	11.3	32.3	11.0	31.3
Bi (%)	1.7	-	1.6	-	1.6	-
B (%)	7.5	9.7	7.4	9.7	7.4	9.4
$\mu_s'(\lambda)$ (cm^{-1})	13.0	15.7	13.0	16.0	13.0	15.8
b	0.3	3.2	0.3	3.2	0.3	3.1
ρ (%)	-	99.9	-	102.1	-	100.0
Total (%)	88.7	127.9	87.9	129.5	87.8	126.5

Discussion

Ex vivo bovine liver

Looking at Fig. 10, it can be concluded that the MC model has larger residues than the DM. In Table 3, however, there does not seem to be any unexpected volume fractions in the MC model. It can be seen that the oxidation level of the blood, for example, is around 10 - 15% according to the MC model, and around 80% according to the DM. In that case, the MC model has the most likely result, since the oxidation level of *ex vivo* tissue is more often around 10% [6]. The water, lipid, bile and blood fractions are more similar for both models and seem realistic compared to the input values in Table 1. The parameters that differ most from Table 1 are the power coefficients for both models, and the lipid fraction in the DM that seems to be too high.

When comparing the total sum of volume fractions of two models, it can be seen that the DM gets a sum around 130% while MC model has a total sum around 95%. Overall, Table 3 indicates that the MC model is better than the DM.

Ex vivo porcine liver

For the porcine liver, the fit of the MC model and DM are equally good. However, the volume fractions of the MC model seem much more realistic than the values from the diffusion model, when compared to the input values. The oxidation level, lipid, blood and water fractions are high for both models compared to previous studies, but the diffusion model gives extremely high values for some of these parameters. For example it gives a water fraction over 100% or an oxidation level at 66% which is unlikely for *ex vivo* tissue. The rest of the parameters for both models seem realistic.

The total sum of the volume fractions are still better for the MC model; the MC model has one spectrum with a sum of about 130 and the other at 102% while the DM has a sum between 130 - 150%.

It is obvious that the *ex vivo* tissue measurements give worse fit than the *in vivo* tissue for both models. This might be due to bad probe handling during the *ex vivo* measurements, that give errors in the spectra. Those errors might then result in strange parameter values.

In vivo human liver

The result of the *in vivo* human liver shows that both models fit the spectra very well and that the DR spectra varies more for *in vivo* measurements than *ex vivo.* The variations are due to more variations in the tissue, such as more blood vessels at certain points, arteries or veins, the fluency of blood and bile and other changes in the tissue. Another contribution to the change may be the probe pressure that changes more due to the respiration of the patient, or due to chemotherapy induced damages as steatosis and steatohepatitis. The variations can be seen for all parameters in Table 4 and 5. The most interesting is that the MC model seems to be able to differ *ex vivo* tissue from *in vivo* tissue on the oxidation level, while the DM cannot.

Most parameters, both for the DM and the MC model, seem quite realistic. The exceptions are the bile fractions in the MC model. The bile fraction that is around 15%, might be a bit high for the MC model; a healthy liver has around 5% bile according to Table 1. Reasons for the high value might be that some water is considered to be bile since bile consists of a lot of water and there therefore are similarities in their absorption spectra.

The variations in volume fractions results in variations in the total sum. In the first occasion, the DM is closer to 100% than earlier, but the MC model is still better. In the second occasion, the models are approximately equally close to 100%.

Probe pressure

The probe-pressure measurements show that humans are able to reproduce a pressure, but that it still is important with training with the probe, earlier experience with the tissue, knowledge about how much pressure that is allowed and how hard pressure one uses. The independent person had very loose pressure, especially during the measurements for the light pressure where the probe was not in contact with the tissue, even though the importance of optical contact had been discussed before the measurements. The idea of training with the probe was strengthened during the *in vivo* measurements. There it could be seen that the surgeons that handled the probe during the surgeries held the probe very stable by looking at the live DR spectrum in Ocean View. Therefore, the stability of the probe should not be a problem, considering that the equipment is aimed to be used during surgeries in the future and therefore constructed to reduce stability problems, and surgeons seem to be very stable with that kind of equipment.

The pressure measurements indicate that a higher pressure would mean a higher reflectance. However, there are different results of how the pressure changes the reflectance. One result according to previous studies [13] and [14], is that the reflectance increases for higher pressures below a so called pivot point at 590 nm, and above that point, the reflectance decreases for higher pressure, while another study [15] shows decreased DR for a higher pressure. The results in this project can be explained by that the highly absorbing chromophores, blood and water, are pressed away resulting in more photons to be collected, causing a higher reflectance. The results in Table 7, shows that the MC model indicates that the volume fraction of lipid, water, bile and blood decreases, while no clear pattern can be seen with the DM.

The results from previous studies, that show an increase below the pivot point, is probably due to a lower fraction of blood as discussed above, but the decrease above that point is harder to explain. An idea by Chan et al [15], is that the pressed away liquid is only free water and decreases the total volume of the liver, so that the volume fraction of water is larger due to the bound water. Another idea is that the differences in the tissue result in a different scattering path of the photons that change the DR spectrum. However, there are too few studies done in this field, mostly concerning pressures that are higher than the ones used in this thesis, to come to any certain conclusions.

The effect of the pressure on the DR spectra does not seem to be very important concerning the capacity to discover tumours and chemotherapy induced damages. Fig. 14 shows, that in these low probe-pressures the shape of the spectrum does not deviate for the different pressures, only the magnitude of DR does. Fig 14 also shows that both models actually match the difference of the DR spectra for the different pressures, i.e. the MC model seems to detect the reflectance difference even though it does not match the actual shape, which indicates that the shortcomings of the model is somewhere in the LUT, or the fit of the LUT. Considering that the shape of the spectrum can vary just between different points in the *in vivo* liver, the shape of the spectra should change more for tumours and chemotherapy induced damages. For steatosis and steatohepatitis for example, the fraction of lipids is much

larger, which means that the absorption would be higher above 1000 nm and therefore the reflectance would be lower above 1000 nm, and the peak at 800 nm should be the peak with the highest reflectance. For tumours, the fraction of bile and blood would be less, and the fraction of water higher. Since blood is highly absorbing below 600 nm, and water is highly absorbing above 1000 nm, the reflectance would increase below 600 nm and decrease above 1000 nm if the collected DR originated from a tumour.

Analysis model

Looking at the results, it is obvious that the model, as it is today, is not good enough to be used as a tool during surgery even though the MC model mostly gives more reasonable results than the DM. However, it is hard to draw any conclusions about which model that is the best since the two models have different sets of parameters. It would be a good idea to try to add bile in the diffusion model, and run it considering only Mie scattering, to get a more clear comparison between the two models. Unfortunately, the shortcoming of the diffusion model, where the DR is modelled to zero in the region above 1400 nm is still present in the Monte Carlo. This can be explained by the fact that there is almost no signal in that region, which makes the polynomial fit sett the function to zero in that region.

The main reason for the bad fit of the MC model in some cases is probably the polynomial fit of the LUT. There are several options when doing the actual matching of the curves, but the polynomial fit was considered to be the best compared to the other options since the chosen optimization routine needs an analytic function, and an analytic function erases the noise in the LUT that would result in sudden extreme deviations from the expected DR curve. However, the polynomial fit differs from the LUT, which probably gives the mismatch of the measured data around 800 nm. An idea would therefore be to find an analytic fit that matches the surface better, or try to come up with an optimization routine that does not need an analytic function. The Levenberg-Marquardt algorithm that was used was not the only option; one could have used another built in routine as Hennessy *et al* [12], a trust-region-reflective algorithm, or write a special optimization routine oneself. The reason for choosing the Levenberg-Marquardt algorithm was simply that one did not have to use constraints of the input parameters there, which could be done in the trust-region-reflective algorithm, and writing an own routine was considered to be too time-consuming in this thesis.

A second improvement to the model, except for a better fit of the LUT, would be to improve the initial LUT, as for example use smaller steps of the coefficients. Another way to create a more accurate LUT, with less fluctuations, is to simulate more photons; the number of photons in this project is just 100 000, but 1 000 000 or 10 000 000 photons would give a smoother LUT. The reason for not simulating more photons is that the simulations take a lot of time; the one used in this project took 6 days, and when a simulation of 10 000 000 photons was run, the computer took over a month to simulate 36 of over 10 000 combinations. The time-consumption could be reduced by using CUDAMCML that can run many simulations in parallel, for example reduce the simulation time with a factor 100 as Alerstam [24].

Conclusions and outlook

The MC model seems to be a promising method of analysing tissue. Since there are known shortcomings of the diffusion model, this model in its present version, is probably a better method than the diffusion model in wavelength regions with highly absorbing chromophores, such as liver. However, both models should use the same input parameters before any conclusions can be drawn.

Neglecting the shortcomings of the diffusion model in certain wavelength regions, both models have some uncertainties; both models sometimes show for example unreasonable parameter values, which might be due to measurement errors. The main mismatch of the MC model as it is today is the high value of the bile fraction, and the fit of the LUT that gives the large residues of the MC model around 800 nm. The bile fraction is hard to manipulate, but the fit of the LUT should definitely be improved. Otherwise, it would be a good idea to use another optimization routine.

Considering the probe-pressure measurement, this work indicates that a higher pressure gives a higher DR, which clearly can be seen in the plots and the results of the MC model, but not in the DM. Due to the uncertainties in the MC model, nothing can be considered to be sure, especially not since there is not many studies done in this field, and the few that are done, shows contradictory results.

Acknowledgements

I would like to thank everyone that has helped me make this project possible. First and foremost I would like to than my supervisors Nina Reistad giving me the possibility to be a part of a larger research project and receiving the results from the diffusion model for me, and Stefan Andersson-Engels for always helping me when I have been stuck in the programming. Further, I would like to thank Åke Johansson for all the help with the computer when I have tried to run too large simulations, and Johan Axelsson for taking the time to help me with programming problems even though he has no obliges to do that.

I would also thank Jan Nilsson, Christian Sturesson, Magnus Bergenfeldt, and the rest of the staff at the hospital for their gentleness an ability to make me feel part of the team and their inspiring teamwork. Finally I would like to thank Jennifer Gustavsson for being a guinea pig with a large amount of patience, my boyfriend Jonas Ravelid, my mother, Johan Zetterberg and all of my friends for their comforting and good advice when I have been stressed.

References

[1] J. Ferlay, I. Soerjomataram, R. Dikshit *et al.*, "Cancer incidence and mortality worldwide: sources, methods and major patterns in GLOBOCAN 2012," International Journal of Cancer, 136(5), E359-E386 (2015).

[2] J. Leporrier, J. Maurel, L. Chiche *et al.*, "A population-based study of the incidence, management and prognosis of hepatic metastases from colorectal cancer," British journal of surgery, 93(4), 465-474 (2006).

[3] G. Steele Jr, and T. Ravikumar, "Resection of hepatic metastases from colorectal cancer. Biologic perspective," Annals of surgery, 210(2), 127 (1989).

[4] P. J. Kneuertz, S. K. Maithel, C. A. Staley *et al.*, "Chemotherapy-associated liver injury: impact on surgical management of colorectal cancer liver metastases," Annals Of Surgical Oncology, 18(1), 181-190 (2011).

[5] Z. Volynskaya, A. S. Haka, K. L. Bechtel *et al.*, "Diagnosing breast cancer using diffuse reflectance spectroscopy and intrinsic fluorescence spectroscopy," Journal of biomedical optics, 13(2), 024012-024012-9 (2008).

[6] R. Nachabé, D. J. Evers, B. H. W. Hendriks *et al.*, "Effect of bile absorption coefficients on the estimation of liver tissue optical properties and related implications in discriminating healthy and tumorous samples," Biomedical Optics Express, 2(3), 600-614 (2011).

[7] D. J. Evers, R. Nachabe, D. Hompes *et al.*, "Optical sensing for tumor detection in the liver," Eur J Surg Oncol, 39(1), 68-75 (2013).

[8] N. Reistad, J. Nilsson, O. Vilhelmsson Timmermand *et al.*, "Diffuse reflectance spectroscopy of liver tissue," Proc. SPIE 9531, Biophotonics South America, 95314E-95314E-10 (2015).

[9] T. Alburg, and D. Kraus, "Diffuse reflectance spectroscopy as a tool to evaluate liver tissue," LUP Student Papers, Lund University, (2014).

[10] T. J. Farrell, M. S. Patterson, and B. Wilson, "A diffusion theory model of spatially resolved, steady-state diffuse reflectance for the noninvasive determination of tissue optical properties in vivo," Medical Physics, 19(4), 879-888 (1992).

[11] N. Rajaram, T. H. Nguyen, and J. W. Tunnell, "Lookup table–based inverse model for determining optical properties of turbid media," Journal of biomedical optics, 13(5), 050501-050501-3 (2008).

[12] R. Hennessy, S. L. Lim, M. K. Markey *et al.*, "Monte Carlo lookup table-based inverse model for extracting optical properties from tissue-simulating phantoms using diffuse reflectance spectroscopy," Journal of Biomedical Optics, 18(3), 037003-037003 (2013).

[13] N. Reistad, M. Mayjonade, A. Ahadi *et al.*, "Characterization of probe contact effects on diffuse reflectance spectroscopy measurements," Proc. SPIE 9531, Biophotonics South America, 953143-953143-8 (2015).

[14] L. L. Randeberg, [Diagnostic applications of diffuse reflectance spectroscopy] Department of Electronics and Telecommunications, Norwegian University of Science and Technology, (2005).

[15] E. K. Chan, B. Sorg, D. Protsenko *et al.*, "Effects of compression on soft tissue optical properties," IEEE Journal of Selected Topics in Quantum Electronics, 2(4), 943-950 (1996).

[16] T. M. Bydlon, R. Nachabé, N. Ramanujam *et al.*, "Chromophore based analyses of steady-state diffuse reflectance spectroscopy: current status and perspectives for clinical adoption," Journal of Biophotonics, 8(1-2), 9-24 (2015).

[17] S. L. Jacques, "Optical properties of biological tissues: a review," Physics in Medicine and Biology, 58(11), R37-R61 (2013).

[18] R. Nachabé, B. H. W. Hendriks, M. van der Voort *et al.*, "Estimation of biological chromophores using diffuse optical spectroscopy: benefit of extending the UV-VIS

wavelength range to include 1000 to 1600 nm," Biomed. Opt. Express, 1(5), 1432-1442 (2010).
[19] R. L. van Veen, A. Amelink, M. Menke-Pluymers *et al.*, "Optical biopsy of breast tissue using differential path-length spectroscopy," Physics in medicine and biology, 50(11), 2573 (2005).
[20] A. Cerussi, N. Shah, D. Hsiang *et al.*, "In vivo absorption, scattering, and physiologic properties of 58 malignant breast tumors determined by broadband diffuse optical spectroscopy," Journal of biomedical optics, 11(4), 044005-044005-16 (2006).
[21] J. Q. Brown, L. G. Wilke, J. Geradts *et al.*, "Quantitative optical spectroscopy: a robust tool for direct measurement of breast cancer vascular oxygenation and total hemoglobin content in vivo," Cancer research, 69(7), 2919-2926 (2009).
[22] R. L. van Veen, H. J. Sterenborg, A. Pifferi *et al.*, "Determination of visible near-IR absorption coefficients of mammalian fat using time-and spatially resolved diffuse reflectance and transmission spectroscopy," Journal of biomedical optics, 10(5), 054004-054004-6 (2005).
[23] S. A. Prahl, M. Keijzer, S. L. Jacques *et al.*, "A Monte Carlo model of light propagation in tissue," Dosimetry of laser radiation in medicine and biology, 5, 102-111 (1989).
[24] E. Alerstam, [Optical spectroscopy of turbid media: time-domain measurements and accelerated Monte Carlo modelling] Lund University, LUP Student Papers (2011).
[25] L. Wang, S. L. Jacques, and L. Zheng, "MCML—Monte Carlo modeling of light transport in multi-layered tissues," Computer Methods and Programs in Biomedicine, 47(2), 131-146 (1995).
[26] R. L. van Veen, W. Verkruysse, and H. J. Sterenborg, "Diffuse-reflectance spectroscopy from 500 to 1060 nm by correction for inhomogeneously distributed absorbers," Optics letters, 27(4), 246-248 (2002).

Appendix

Matlab codes

Forward model

```
% Creation of wavelength dependent mu_a and mu_s (step 2)
% Uses values for the different chromophore absorption coefficients
% from 'Nachabe et al. Opt. Express 18(24), 2010' loaded in
"chromophoreabsorptionB.mat"

% Uses initial volume fraction guesses (parameters that should be updated
% with the search routine) from 'Nachabe et al.2011'

% Created: spring 2015 by Alexandra Andersson

clear all
close all

load('chromophoreabsorptionB.mat');

% Input parameters

R_vessel = 53*10^(-4);     % Radius of blood vessel ([cm])
S = 0.08;    %pm14         % Saturation level of blood (%)
W = 0.76;    %pm4          % Volume fraction of water (%)
L = 0.16;    %pm3          % Volume fraction of Lipids (%)
Bi = 0.055; %pm2.3         % Volume fraction of Bile (%)
B = 0.032;  %pm1.6         % Volume fraction of Blood (%)

mu_s0 = 17;  %pm3          % Scattering coefficient at reference wavelength
                           ([cm^(-1)])
lam_ref = 800;             % Reference wavelength (nm)
b = 1.2; %pm07             % slope of Mie reduced scattering (between 0 and
                           4)

% Absorption

wl = chrom.wl;               % Wavelength from chromophoreabsorptionB.mat
                             (430-1590 nm)
mu_Hb = chrom.hb;            % Abs coeff for deox Hb
mu_HbO2 = chrom.hbo2;        % Abs coeff for ox Hb
mu_H2O = chrom.water;        % Abs coeff for Water
mu_Lipid  = chrom.lipid;     % Abs coeff for Lipids
mu_Bile = chrom.bile;        % Abs coeff for Bile

% Correction term

C_diff = (1 - exp(-2.*R_vessel.*(S.*mu_HbO2 + (1-
S).*mu_Hb))./(2.*R_vessel.*(S.*mu_HbO2 + (1-S).*mu_Hb));
```

```
Rest_of_chrom = W.*mu_H2O + L.*mu_Lipid + Bi.*mu_Bile;

mu_a_blood = C_diff.*(B.*(S.*mu_HbO2 + (1-S).*mu_Hb));

mua = (mu_a_blood + Rest_of_chrom);

% Scattering

musp = mu_s0.*((wl./lam_ref).^(-b));

% Plot all abs coeff for the different chromophores

figure('position',[100 100 1000 700])
semilogy(wl,mu_Hb, 'b-')
hold on
semilogy(wl,mu_HbO2, 'r-')
hold on
semilogy(wl,mu_H2O, 'k-')
hold on
semilogy(wl,mu_Bile, 'm-')
hold on
semilogy(wl,mu_Lipid, 'g-')
xlabel('Wavelength (nm)', 'FontSize', 18)
ylabel('Absorption coefficient (cm^{-1})', 'FontSize', 18)
title('Chromophore absorption', 'FontSize', 18)
a = legend('Hb', 'HbO_{2}','H_{2}O','Bile','Lipid');
LEG = findobj(a,'type','text');
set(LEG,'FontSize',16)

% Plot scat and abs coeff

figure('position',[100 100 1000 700])
semilogy(wl,mua,'r-')
hold on
semilogy(wl,mus,'b-')
xlabel('Wavelength (nm)','FontSize', 18)
ylabel('Absorption and reduced scattering coefficient (cm^{-
1})','FontSize', 18)
title('Absorption and reduced scattering coefficients','FontSize', 18)
b = legend('\mu_a', '\mu^{´}_s');
LEG = findobj(b,'type','text');
set(LEG,'FontSize',16)
```

Creation of Look-up table

```
% Creation of Lookup-table (step 1)
% File that creates a Lookup-table, using two modified files; MCML_mod.m
and create_MCML_input_file_mod.m
% Save reflectance for every run and plot the 3D plot for a specific
% interesting radius r. (r equal to 0.25 cm )
% Add from r = 0.23 cm to r = 0.27

% Created: spring 2015 by Alexandra Andersson
```

```
i_max = 70;
j_max = 151;

layers_matrix = zeros(i_max,j_max,5);

Saved_Ref_LUT = zeros(i_max,j_max,30);


for i = 1:i_max

    for j = 2:j_max

    log_mua(i) = 0.1*i - 2.6;
    mu_a(i) = exp(log_mua(i));

    mu_s(j) = j-1;

    n = 1.4; %Refractive index
    g = 0.85;
    thickness = 100; % Thick enough to not let any photons through

    layers_matrix(i,j,:) = ([n, mu_a(i), mu_s(j), g, thickness]);
    s = MCML_mod('LUT',1000,layers_matrix(i,j,:));

    Saved_Ref_LUT(i,j,:) = ([s.refl_r]);

 end

end

Ref_LUT = Saved_Ref_LUT(:,:,23) + Saved_Ref_LUT(:,:,24) +
Saved_Ref_LUT(:,:,25) + Saved_Ref_LUT(:,:,26) + Saved_Ref_LUT(:,:,27);

mus = mu_s(1:75);
musp = mus.*(1-g);
mua = log(mu_a);

Ref = Ref_LUT(:,1:75,:);

figure('position',[100 100 1000 700])
mesh(Ref)
title('Lookup-table', 'FontSize', 18)
ylabel('Step of \mu_a (cm^{-1})', 'FontSize', 18)
xlabel('Step of \mu_s (cm^{-1})', 'FontSize', 18)
zlabel('Diffuse Reflectance', 'FontSize', 18)

% Fit of LUT

p00 =    0.009521;
p10 =    0.003205;
p01 =     0.08546;
p20 =     -0.0164;
p11 =     -0.0949;
p02 =     0.04441;
p30 =    0.003194;
p21 =    0.006215;
p12 =    -0.01132;
p03 =   -0.007291;
```

```
p40 =    0.003072;
p31 =    0.006799;
p22 =   0.0004938;
p13 =    0.001751;
p04 =    0.000415;
p50 =  -0.0007379;
p41 =  -0.0008679;
p32 =  -0.0001389;
p23 =  -3.125e-05;
p14 =  -6.306e-05;
p05 =  -7.954e-06;


% Plotting the spectra

 for i = 1:70
    for j = 1:75

        log_mua(i) = 0.1*i - 2.6;
        x(i) = log_mua(i);

        y(j) = j-1;
        y(j) = y(j).*(1-g);

Opt_ref(i,j) = p00 + p10*x(i) + p01*y(j) + p20*x(i)^2 + p11*x(i)*y(j)+
p02*y(j)^2 + p30*x(i)^3 + p21*x(i)^2*y(j)+ p12*x(i)*y(j)^2 + p03*y(j)^3 +
p31*x(i)^3*y(j)+ p22*x(i)^2*y(j)^2 + p13*y(j)^3*x(i)+ p04*y(j)^4+
p32*x(i)^3*y(j)^2 + p23*x(i)^2*y(j)^3 + p14*x(i)*y(j)^4 + p05*y(j)^5+
p40*x(i)^4 + p50*x(i)^5 + p41*x(i)^4*y(j);

    end
 end

res = Ref - Opt_ref;

figure('position',[100 100 1000 700])
mesh(Opt_ref)
title('Polynomial fit of Lookup-table', 'FontSize', 18)
ylabel('Step of log(\mu_a) (cm^{-1})', 'FontSize', 18)
xlabel('Step of \mu^{´}_s (cm^{-1})', 'FontSize', 18)
zlabel('Diffuse Reflectance', 'FontSize', 18)

figure('position',[100 100 1000 700])
mesh(res)
title('Residue of polynomial fit', 'FontSize', 18)
ylabel('Step of log(\mu_a) (cm^{-1})', 'FontSize', 18)
xlabel('Step of \mu^{´}_s (cm^{-1})', 'FontSize', 18)
zlabel('Diffuse Reflectance', 'FontSize', 18)

figure('position',[100 100 1000 700])
plot(mu_a,'r')
hold on
plot(mua,'m')
hold on
plot(mus,'b')
hold on
plot(musp,'k')
title('Coefficient values in LUT')
xlabel('Step','FontSize', 18)
```

```
ylabel('Coefficients (cm^{-1})','FontSize', 18)
title('Coefficients','FontSize', 18)
b = legend('\mu_a','log(\mu_a)','\mu_s','\mu^{´}_s');
LEG = findobj(b,'type','text');
```

Inverse model

```
% Inverse model (step 4)

% Minimize the difference between measured spectrum and the modelled
spectrum
% Created: spring 2015 by Alexandra Andersson
% Calls function "Inverse", and optimize the input parameters x0

clear all
close all

x0=[0.08,0.76,0.16,0.05,0.032,17,1.2];
LB=[0,0.3,0.01,0.0001,0.0001,5,1];
UB=[1,0.95,0.5,0.30,0.15,50,4];

OPTIONS = optimoptions('fsolve','Algorithm','levenberg-marquardt');
Optimized_parameters = fsolve(@(x) Inverse(x),x0,OPTIONS);


function [ delta ] = Inverse(x)

load('chromophoreabsorptionB.mat');
load('Press.mat');

% If Porcine_2: use R2 and R5
% If Bovine_2: use R1and R4
% If Press: use HR, MR and LR
% If Liver1: use R1 and R3
% If Liver2: use R7 and R8

lam_ref = 800;
R_vessel = 53*10^(-4);

S = x(1);
Wa = x(2);
L = x(3);
Bi = x(4);
B = x(5);

mu_s0 = x(6);
b = x(7);

% Absorption
% Those parameters are not supposed to be updated!!

wl = chrom.wl;              % Wavelength from chromophoreabsorptionB.mat)
                            (430-1590 nm)
mu_Hb = chrom.hb;           % Abs coeff for deox Hb
mu_HbO2 = chrom.hbo2;       % Abs coeff for ox Hb
mu_H2O = chrom.water;       % Abs coeff for Water
```

```
mu_Lipid  = chrom.lipid;    % Abs coeff for Lipids
mu_Bile = chrom.bile;       % Abs coeff for Bile

% Correction term

C_diff = (1 - exp(-2.*R_vessel.*(S.*mu_HbO2 + (1-
S).*mu_Hb))./(2.*R_vessel.*(S.*mu_HbO2 + (1-S).*mu_Hb));

Rest_of_chrom = Wa.*mu_H2O + L.*mu_Lipid + Bi.*mu_Bile;

mu_a_blood = C_diff.*(B.*(S.*mu_HbO2 + (1-S).*mu_Hb));

mua = (mu_a_blood + Rest_of_chrom);

mua = mua(146:1071);


% Scattering

musp = mu_s0.*((wl./lam_ref).^(-b)); % + (1-rho).*((wl./lam_ref).^(-4)));

musp = musp(146:1071);

Opt_meas = interp1(HW,HR,wl,'spline');
Opt_meas = Opt_meas(146:1071);
wl = wl(146:1071);

% Fit of LUT

p00 =    0.009521;
p10 =    0.003205;
p01 =     0.08546;
p20 =     -0.0164;
p11 =     -0.0949;
p02 =     0.04441;
p30 =    0.003194;
p21 =    0.006215;
p12 =    -0.01132;
p03 =   -0.007291;
p40 =    0.003072;
p31 =    0.006799;
p22 =   0.0004938;
p13 =    0.001751;
p04 =    0.000415;
p50 =  -0.0007379;
p41 =  -0.0008679;
p32 =  -0.0001389;
p23 =  -3.125e-05;
p14 =  -6.306e-05;
p05 =  -7.954e-06;


% Plotting the spectra

for k = 1:926

xx(k) = log(mua(k));
yy(k) = musp(k);
```

```
Opt_ref(k) = p00 + p10*xx(k) + p01*yy(k) + p20*xx(k)^2 + p11*xx(k)*yy(k) +
p02*yy(k)^2 + p30*xx(k)^3 + p21*xx(k)^2*yy(k)+ p12*xx(k)*yy(k)^2 +
p03*yy(k)^3 + p40*xx(k)^4 + p31*xx(k)^3*yy(k) + p22*xx(k)^2*yy(k)^2 +
p13*xx(k)*yy(k)^3 + p04*yy(k)^4+ p50*xx(k)^5 + p41*xx(k)^4*yy(k) +
p32*xx(k)^3*yy(k)^2 + p23*xx(k)^2*yy(k)^3 + p14*xx(k)*yy(k)^4 +
p05*yy(k)^5;

end

maxy = max(Opt_meas);
index = find(Opt_meas == maxy);
XP = wl(index) - 574;

MCmod = Opt_ref';
rat1 = Opt_meas(XP)./MCmod(XP);
MCmod = rat1.*MCmod;

delta = MCmod - Opt_meas;

end
```